Desalination 572 (2024) 117108

Contents lists available at ScienceDirect

Desalination

journal homepage: www.elsevier.com/locate/desal

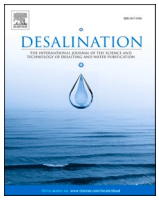

Selective recovery of silver ions from copper-contaminated effluents using electrodialysis

Pauline Zimmermann [a], Kristin Wahl [b], Önder Tekinalp [c], Simon Birger Byremo Solberg [a], Liyuan Deng [c], Øivind Wilhelmsen [d], Odne Stokke Burheim [a,*]

[a] Department of Energy and Process Engineering, Norwegian University of Science and Technology (NTNU), NO-7491 Trondheim, Norway
[b] Department of Materials Science and Engineering, Norwegian University of Science and Technology (NTNU), NO-7491 Trondheim, Norway
[c] Department of Chemical Engineering, Norwegian University of Science and Technology (NTNU), NO-7491 Trondheim, Norway
[d] Department of Chemistry, Norwegian University of Science and Technology (NTNU), NO-7491 Trondheim, Norway

HIGHLIGHTS

- Selective separation of Ag^{+} and Cu^{2+} via electrodialysis was studied at varying pH.
- up to 80 % separation efficiency and complete removal of Ag^{+} was achieved.
- Limiting current density increased with pH.
- Lower pH had a detrimental effect on energy efficiency.
- Energy efficiency increased from 2 % at pH 1 to 37 % at pH 4.5.

GRAPHICAL ABSTRACT

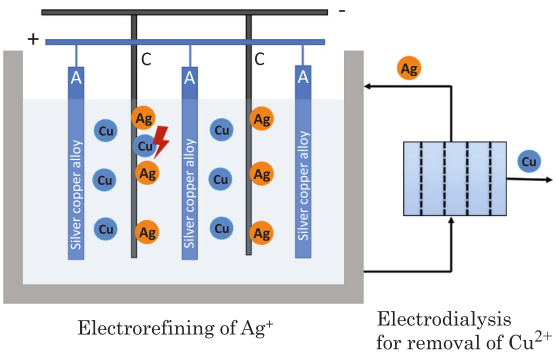

ARTICLE INFO

Keywords:
Electrodialysis
Monovalent selectivity
Concentration polarization
Limiting current density
Ion-exchange membranes

ABSTRACT

With the growing demand for silver, the recycling of this precious metal from secondary sources has become imperative. However, the presence of copper impurities poses a significant challenge. This study aims to explore electrodialysis for selectively recovering silver ions from copper-contaminated effluents, elucidating the effect of low pH on the process performance. Electrodialysis of 10 mM equimolar solutions of silver nitrate and copper nitrate was performed at various pH levels, using nitric acid for pH adjustment. Adjusting the operational current to the limiting current resulted in similar silver fluxes and copper leakages at pH 1, 2, and 4.5. The energy requirement was governed by proton abundance, competing with silver ions for charge transport in the electrodialysis cell. The specific energy consumption for silver removal decreased from 751 kJ/mol at pH 1 to 36 kJ/mol at pH 4.5, with the energy efficiency rising from 2 % at pH 1 to 37 % at pH 4.5. Copper leakage was approximately 20 % in all cases, yielding silver-copper separation efficiencies of 55 % at pH 1 and 80 % at pH 2 and 4.5. This study highlights electrodialysis as a promising technique for purifying hydrometallurgical effluents, emphasizing the need for case-specific assessment depending on feed water properties. Notably, the limitations associated with low pH suggest potential advantages of adjusting the pH of the solution.

* Corresponding author.
E-mail address: burheim@ntnu.no (O.S. Burheim).

https://doi.org/10.1016/j.desal.2023.117108
Received 4 September 2023; Received in revised form 20 October 2023; Accepted 25 October 2023
Available online 4 November 2023

1. Introduction

Precious and noble metals, such as silver, gold, and the platinum group metals, are rare elements that possess high economic value due to their scarcity and exceptional chemical properties, including resistance to oxidation and corrosion [1]. Among these metals, silver stands out as the most versatile, renowned for its excellent electrical and thermal conductivity, durability, and biocompatibility. Consequently, silver finds applications in various industries, including catalysts, electronic devices, jewelry fabrication, and medical purposes [2]. However, with the advancements of the industrialized world, the high demand for silver and its limited availability lead to a deficit in silver supply, necessitating efforts to explore new sources and emphasize recycling [3]. Extraction and recovery of silver have been extensively investigated through hydrometallurgical and biometallurgical approaches [5]. In the hydrometallurgical route, leaching serves as the initial step, followed by the recovery of silver using various techniques such as cementation, chemical precipitation, adsorption, biosorption, electrocoagulation, electrowinning, ion exchange, and solvent extraction [1,3,6]. These techniques play a crucial role in achieving cost-effective silver recovery and extraction from diverse secondary sources. The wide range of origins and composition of silver-containing materials pose significant challenges during their processing [3]. Processes like electrorefining yield silver products of high purity despite the presence of various impurities in secondary silver sources. However, achieving a high-quality product requires meticulous process control, the addition of chemicals, and/or frequent replenishment of process solutions, consequently resulting in the generation of substantial waste streams that need subsequent treatment [6]. Copper is a prevalent impurity in the electrorefining of silver due to its frequent occurrence in silver alloys [7]. During the electrorefining, the anode plates made of secondary silver sources are progressively consumed, resulting in the dissolution of metal ions. A suitable voltage is applied across the cell to cause oxidation of silver metal at the anode and reduction of Ag^+ to form silver metal at the cathode. Less noble metals than silver, with a lower reduction potential, dissolve at the anode but do not plate at the cathode. While silver metal is electroplated onto the cathode and collected by scraping, copper ions accumulate in the solution. With increasing copper concentration, the likelihood of copper deposition rises. Consequently, to uphold a high purity level of the silver product, it becomes necessary to frequently renew the nitric acid solution, leading to significant acid consumption and the generation of substantial waste streams.

An electrodialysis setup in parallel to the silver electrorefining bath presents a possible solution to the copper accumulation. Using monovalent selective cation exchange membranes (mCEMs) enables the separation of silver ions from divalent impurities. By alternating normal-grade anion-exchange membranes (AEMs) and mCEMs between electrodes and applying an electric potential across the cell, anions and monovalent cations are transported across the AEMs and mCEMs, respectively. These ions are accumulated in one compartment, while copper is retained. This process is schematized in Fig. 1 with one cell pair, comprising one AEM, one silver-depleted compartment, one mCEM, and one silver-enriched compartment. Typically, industrial size electrodialysis stacks employ around 100 cell pairs [8,9]. The continuous electrodialysis step facilitates the recycling of a silver-enriched stream back into the electrorefining bath while simultaneously generating a silver-depleted waste stream. The incorporation of electrodialysis offers the advantage of continuous replacement of the nitric acid solution, eliminating the need to frequently halt the electrorefining process and completely replace the bath. Furthermore, this technique ensures a more consistent and stable process, maintaining constant concentrations of silver and copper, thus enabling production with a sustained level of purity. The resultant waste stream facilitates the recycling of other metals, such as copper.

Commercial monovalent-selective membranes, such as Neosepta CXP-S used in this study, are typically fabricated by coating a thin polymer layer on top of normal-grade membranes, which have the same charge as the counter-ion. The charged layer exerts a repelling effect that allows the passage of monovalent counter-ions but significantly restricts the passage of counter-ions of higher valence [10–12]. Apart from the electrostatic barrier effect, selectivity for monovalent over multivalent ions can be enhanced by size-exclusion. A sieving effect can be achieved by creating a dense membrane matrix with narrow pores, or by coating a dense layer on an IEM [11]. Counter-ion selectivity can also be modified by adjusting the ion hydrophobicity, as ions have been shown to carry an ion-specific and membrane-dependent hydration shell through the membranes [13–16]. Additionally, determining the limiting current density is crucial for optimizing counter-ion selectivity, as the ratio of applied current to limiting current dictates the mass transport regime [11,17,18]. A loss of selectivity has been reported for monovalent-selective IEMs when operating close to or above the limiting current density [12,19–22]. Neosepta CXP-S is a homogeneous mCEM with high mechanical strength. The styrene based copolymer is functionalized with negatively charged sulfonated groups that facilitate the transport of

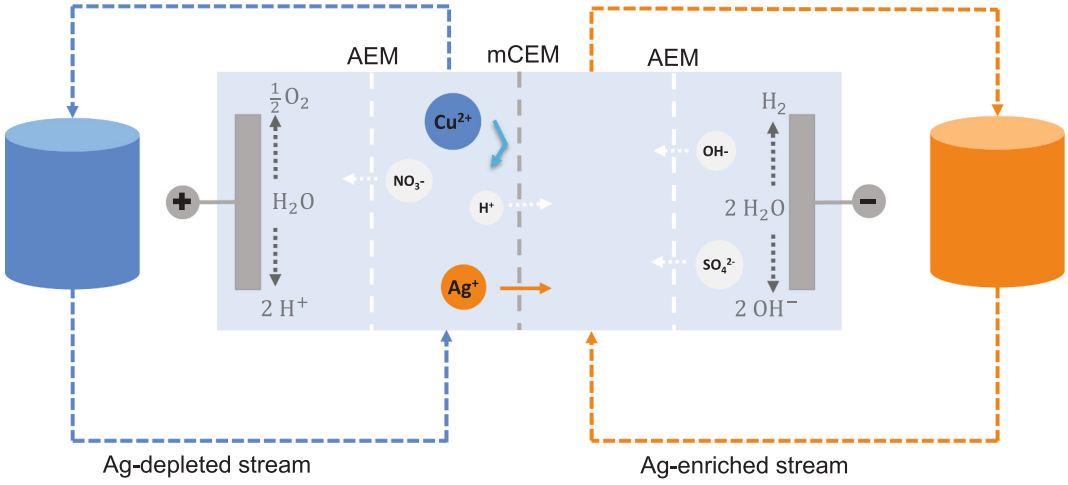

Fig. 1. Schematic description of an electrodialysis cell for the separation of Cu^{2+} and Ag^+ with a single cell pair consisting of an AEM, a silver-depleted compartment, a mCEM, and a silver-enriched compartment. Silver migrates through the mCEMs into the silver-enriched compartment, while copper is retained to a large extent. Protons may also transport through the mCEMs.

cations while repelling anions [23]. Several groups have studied the separation of monovalent from divalent cations using Neosepta mCEMs [12,19,20,24–27] and other commercially available mCEMs [19,21,28–30], as well as layer-by-layer modified membranes [31–39]. The overwhelming majority of the available literature on selective separation of monovalent from divalent metals with electrodialysis explores the separation of alkali metals (specifically Li^+, Na^+, and K^+) from alkaline earth metals (specifically Mg^{2+} and Ca^{2+}). These include the prevalent cationic species found in sea water and other natural water sources, while studies on selective removal of heavy, transition and precious metals with electrodialysis are scarce [1,40,41]. In the hydrometallurgical sector, electrodialysis offers significant benefits to conventional treatments such as precipitation, adsorption, coagulation-flocculation, and solvent extraction. For the recovery of valuable components, the high selectivity offered by functionalized membranes is of major importance. For the removal of impurities from process streams, electrodialysis excels with its chemical-free operation and the absence of solid waste or sludge generation containing hazardous or unstable components that require disposal [15,42,43]. In general, electrodialysis can be employed for treating large volumes of effluents containing low concentrations of specific ions within a short period of time [44]. Salt concentrations between 0.01 and 0.5 M are considered most suitable for the economical operation of electrodialysis, although depending on the individual nature of the process and components [9]. In terms of selective heavy metal removal from industrial process streams, electrodialysis has been employed to separate arsenic from copper and zinc in acidic metallurgical process streams [46] and to separate Cr^{3+} from Na^+ in solutions mimicking wastewaters from lather tanning processes [47]. Vallois et al. [48] studied the separation of Cu^{2+} from H+ for acid recovery. They restricted the passage of Cu^{2+} by coating a commercial Nafion CEM with a thin layer of the positively-charged polymer polyethylene imine (PEI). The membrane modification resulted in a reduction of the copper transport number by up to 74 %. Regarding the selective recovery of precious metals from multi-ionic solutions, electrodialysis has been studied in combination with liquid membranes to separate palladium and platinum [49] and iron and platinum [50]. In liquid membranes, carriers in an organic solvent facilitate the transport of ions from one solution to the other [49]. Recently, Rezaei et al. [51] proposed electrodialysis to recovery gold from electroplating baths, where gold can be separated from other metals because it forms stable anionic complexes with Cl^-.

Similarly, for selective separation of Ag^+ from Zn^{2+} and Cu^{2+} using electrodialysis, the literature presents two relevant studies which are both employing chelating agents to form negatively charged species with the divalent cations [52,53]. Due to the opposite charge signs, silver ions were accumulated on the cathodic side, while the chelated divalent cations were obtained at the anodic side of the membrane stack. Cherif et al. [52] studied the separation of 10 mM mixtures of Ag^+ and Zn^{2+} in nitric acid solution at pH 2.45, using Neosepta mCEMs. A low current efficiency of 10 % for silver recovery was ascribed to the abundance of H^+, which exhibits a high mobility in the CEM. The diffusion coefficients for 50 mM silver, hydrogen, and zinc, each prepared from the nitrate salt, in Neosepta C.M.S. membranes, were determined as $D_{Ag^+} = 3.47{\cdot}10^{-7}\mathrm{cm}^2{\cdot}\mathrm{s}^{-1}$, $D_{Zn^{2+}} = 0.46{\cdot}10^{-7}\mathrm{cm}^2{\cdot}\mathrm{s}^{-1}$, and $D_{H^+} = 17.81{\cdot}10^{-7}\mathrm{cm}^2{\cdot}\mathrm{s}^{-1}$. On the other hand, Güvenç et al. [45] investigated the electrodialytic recovery of 1 mM silver ions under different applied pH levels, and found that the pH had a negligible impact on the removal rate and energy consumption. The pH was adjusted with nitric acid, and the values tested were 2.5, 5, and 7.8.

While chelation-assisted electrodialysis has shown promise in selectively separating silver from metal impurities of higher valence, its efficacy faces limitations due to factors such as the restricted mobility of metal complexes, limited complexation capacities, and the pH-dependent nature of complete chelation [52]. Accordingly, the primary objective of this study is to assess the potential for selectively separating silver from copper ions using electrodialysis with mCEMs while avoiding the need for chelation. To evaluate how the availability of H^+ ions impacts separation performance and energy efficiency, electrodialysis is performed in nitric acid solutions spanning pH levels from 1 to 4.5. The limiting current density for $AgNO_3$ at various pH levels is approximated experimentally and informs the choice of operating current for promoting Ag^+ selectivity. Additionally, the extent of membrane scaling and fouling is analyzed by conducting mass balance calculations.

2. Materials and methods

2.1. Materials

Neosepta ASE (standard grade AEM) and CXP-S (monovalent-selective mCEM) ion-exchange membranes were utilized for all experiments (Eurodia Industries SAS, France). According to the technical specifications, the electrical resistances and thicknesses of the wet membranes are 2.0 cm^2 and 0.10 mm for the CEM, and 2.6 cm^2 and 0.15 mm for the AEM. The electric resistance was measured on alternative current after equilibration with a 0.5 N NaCl solution at 25 °C. The membranes are recommended for use within the whole range of pH (pH 0 to 14) [54]. The active surface area per membrane was 36 cm^2. The membranes were stored in 10 mM silver nitrate solution. Woven silicone/polyester spacers with integrated gaskets were supplied by FumaTech (Germany), with a thickness of 470 μm, a mesh size of 800 μm, and a shadow effect of 0.33, according to supplier information. Solutions were prepared using distilled water and technical grade sodium sulfate (Na_2SO_4) provided by Honeywell International Inc., copper nitrate trihydrate ($Cu(NO_3)_2{\cdot}_3H_2O$) and silver nitrate ($AgNO_3$) provided by Sigma Aldrich. Shenchen V6-6L peristaltic pumps (Baoding Shenchen Precision pump Co., Ltd., China) recirculated the solutions. Concentrated nitric acid (HNO_3) provided by Sigma Aldrich, was utilized for lowering the solution pH. Silver and copper concentrations were measured using microwave plasma atomic emission spectrometry (MP-AES). Standards for the MP-AES analyses were prepared using milli-Q water and inductively coupled plasma (ICP) multi-element standard solution, provided by Merck. As a power supply and for electrochemical measurements, the Gamry Interface 5000E potentiostat/galvanostat and respective Gamry software were used (Gamry Instruments, USA). Methylene blue was used for staining experiments.

2.2. Experimental setup

A customized cross-flow electrodialysis stack with an electrode area measuring 9 × 4 cm^2 was utilized. For each experiment, four cell pairs consisting of an AEM, a silver-depleted compartment, a mCEM, and a silver-enriched compartment were arranged between the electrodes. An additional AEM was placed neighboring the cathode to prevent silver from leaking into the rinse solution. Spacers were inserted between the membranes to facilitate solution flow and mixing. End spacers were placed between the electrodes and the neighboring AEMs to create a closed circuit for rinsing the electrodes. A 500 mL batch of 0.2 M Na_2SO_4 solution served as the rinse solution for each electrode, circulating through the electrode compartments at a flow rate of 100 mL/min. The cell operated in batch mode with 250 mL of feed solution of the same initial composition recirculated trough both compartments. Upon drawing a current, silver gradually transported from the silver-depleted to the silver-enriched batch. Each batch was stirred using a magnetic stirrer. To measure the current-voltage characteristics, a four-electrode configuration was employed, with the working sense and counter sense connected to the stack electrodes. Reference electrodes (Gamry-supplied mercury-sulfate electrodes) were placed in the rinse solutions.

2.2.1. Limiting current density

Limiting current density experiments were performed using the boundary-layer method [55]. Feed solutions of 10 mM, 20 mM, and 30 mM silver nitrate were used without pH adjustment, resulting in a pH of 4.5, and with acidifying the solutions to pH levels of 1, 2, and 3. The solutions were circulated through the electrodialysis stack at a flow rate of 100 mL/min, resulting in a surface velocity of 2.2 cm/s. Amperodynamic sweeps were performed, starting from zero current (open circuit potential). The current was increased in 2–3 mA steps for the solution at pH 4.5, in 5–10 mA steps for the solutions at pH 2 and 3, and in 15–30 mA steps for the solutions at pH 1, until the current reached a maximum value. Each current value was held for 30 s, and measurements of current and voltage were recorded every 0.25 s.

After three-quarters of each current step (once the voltage value had stabilized), the voltage value was plotted against the respective current to obtain the current-voltage characteristics from the experimental data. At low current densities, i.e., in the ohmic region, the current-voltage curves follow a linear trend. However, with increasing current densities, the current-voltage-curve starts to deviate from linearity due to the rise of concentration polarization, which has a detrimental effect on the stack resistance. The deviation between the measured potential, ΔE^{cell}, and the linear extrapolation of the curve in the ohmic regime provides an estimate for the concentration polarization overpotential, ΔE^{CP}. The difference in ion activity at the membrane surface and in the bulk solution, which is a consequence of concentration polarization, can be approximated from ΔE^{CP} by applying the Nernst equation:

$$\Delta E^{\mathrm{CP}} = \mathrm{n}\frac{RT}{|z_i|F} ln\left(\frac{a_i^{\mathrm{surf}}}{a_i^{\mathrm{bulk}}}\right) \tag{1}$$

where z_i is the charge number of ionic species i as an absolute value (i.e., z = 1 for silver), F ($\mathrm{C{\cdot}mol^{-1}}$) is the Faraday constant, n is the number of membranes used in the stack, R ($\mathrm{J{\cdot}K^{-1}{\cdot}mol^{-1}}$) is the universal gas constant, T (K) is the solution temperature, a_i^{surf} and a_i^{bulk} ($\mathrm{mol^{-1}{\cdot}L}$) are the surface and bulk activities of species i, respectively. The activity is defined as $a_i = \gamma_i c_i$, where γ_i and c_i are the activity coefficient and concentration of species i, respectively.

After determining ΔE^{CP} from the deviation between the linear contribution to the cell potential and the measured electric potential, Eq. (1) can be solved for the activity ratio between the solution at the membrane surface and in the bulk. The obtained ratio $\frac{a_i^{\mathrm{surf}}}{a_i^{\mathrm{bulk}}}$ represents an average for all nine diffusion boundary layers facing the silver-depleted side. The limiting current density value was defined as the point where $\frac{a_i^{\mathrm{surf}}}{a_i^{\mathrm{bulk}}} < 0.01$.

2.2.2. Desalination experiments

Electrodialysis was performed with mixtures of 10 mM silver nitrate and 10 mM copper nitrate, following the research done on electrodialytic separation of silver and zinc described in the introduction [52]. The initial pH was adjusted with nitric acid. The current density (j) was set to 20 % of the limiting current density determined for silver nitrate and was held constant throughout the experiment. The relatively low current was chosen because the current was not dynamically adjusted during the experiments to match the decreasing concentration in the silver-depleted compartment, leading to an increasing ratio of drawn current to limiting current during the experiment. Desalination experiments were run for 2 h or until reaching an electric potential that exceeded the maximum potential of around 6 V sustained by the Gamry potentiostat. 5 mL samples were taken regularly from the silver-enriched and silver-depleted compartments to determine the silver and copper concentrations. In addition, the current density and voltage were recorded when taking a sample.

The silver and copper fluxes were calculated based on their concentration change per time step [56]:

$$J_i(n_t) = \frac{V(n_t)}{A}\cdot\frac{c_i(n_t) - c_i(n_t-1)}{t(n_t) - t(n_t-1)} \tag{2}$$

where V (L) is the solution volume on the silver-depleted side, A ($\mathrm{m^2}$) is the active area of the membranes, c_i is the concentration of species i ($\mathrm{mol{\cdot}L^{-1}}$), n_t is the time step, and t is the time (s). The volume change due to sample taking was considered in the flux calculation. However, the water drag from the silver-depleted to the silver-enriched compartments was neglected.

The specific energy consumption, or work input, per mol of silver removed from the silver-depleted batch, W_{Ag}^{spec}, was calculated as follows:

$$W_{Ag}^{spec}(n_t) = \frac{\Delta E^{cell}(n_t) I[t(n_t) - t(n_t-1)]}{[c_i(n_t) - c_i(n_t-1)]V(n_t)} \tag{3}$$

where ΔE^{cell} is the electric potential across the electrodialysis stack (V) and I is the electric current (A).

The energy efficiency based on the second law of thermodynamics is assessed by relating the Gibbs free energy corresponding to the measured change in chemical potential of silver, ΔG_{Ag}, to the spent energy in the system, W_{el}, according to [57]:

$$\eta = \frac{|\Delta G_{Ag}|}{W_{el}}\cdot 100 \tag{4}$$

where $W_{el} = \int_0^t \Delta E^{cell} I \mathrm{d}t$. ΔG_{Ag} is defined as:

$$\Delta G_{Ag} = RTVc_{\mathrm{Ag}}^{HC} ln\left(\frac{a_{\mathrm{Ag}}^{LC}}{a_{\mathrm{Ag}}^{HC}}\right) \tag{5}$$

Given the low concentrations of silver, the activity coefficients are taken to be unity, and therefore $a_i = c_i$.

To quantify the relative difference in transport rate between the competing counter-ions, the separation efficiency, S_B^A, as introduced by van der Bruggen et al. [30], is used:

$$S_{Cu}^{Ag}(n_t) = \frac{\left[\frac{c_{Cu}(n_t)}{c_{Cu}(n_t-1)}\right] - \left[\frac{c_{Ag}(n_t)}{c_{Ag}(n_t-1)}\right]}{\left[1 - \frac{c_{Cu}(n_t)}{c_{Cu}(n_t-1)}\right] + \left[1 - \frac{c_{Ag}(n_t)}{c_{Ag}(n_t-1)}\right]} \tag{6}$$

where c_{Cu} and c_{Ag} are the concentration of silver and copper ions in the silver-depleted compartment, respectively. S_{Cu}^{Ag} ranges from −1 (complete selectivity for copper) to 1 (complete selectivity for silver).

The increasing ion concentration in the concentrate compartment of an electrodialysis stack, combined with concentration polarization at the membrane-solution interface and the generation of hydroxide ions at the cathode and membrane surface due to water splitting, can lead to scaling of metal ions during the electrodialysis process [59]. This phenomenon poses a significant drawback in maintaining continuous and smooth operation of electrodialysis. The precipitation of minerals inside the electrodialysis unit, specifically at the membrane surfaces, has detrimental effects on the process performance, causing a substantial and often irreversible increase in the stack's electrical and hydraulic resistance [9]. To quantify the loss of silver and copper in the solutions due to scaling, mass balances were assessed by weighing the silver-depleted and silver-enriched containers before and after desalination to determine the change in the amount of substance according to the measured concentrations. The amount of silver and copper taken out for sampling was considered in these calculations. The solution density was assumed to be 1 g/L. The concentrations of silver and copper in the rinse solutions before and after the experiments were also determined, to ensure that no significant amount of silver and copper was dragged into the electrode compartments during the experiments. To determine the possible silver and copper species present in the feed solution, a speciation model was prepared using *Visual MINTEQ* software [62]. The

Davies model [63] was utilized to calculate activities within the electrolyte.

3. Results and discussion

3.1. Limiting current density

Fig. 2 shows the plots of the current-voltage characteristics, overpotential, and activity ratio at the membrane surface and in the bulk solution for silver nitrate solutions of 10 mM, 20 mM, and 30 mM at pH 1. Respective plots for the pH levels 2, 3, and 4.5 can be found in Appendix A. Each experiment was repeated once, and the full and hollow symbols represent repetitions at the same conditions. Results for limiting current densities at different silver nitrate concentrations and pH levels are presented in Fig. 3 with respective error estimates.

Fig. 3 demonstrates a direct relationship between the silver nitrate concentration and the limiting current density within the tested concentration range, evident across the applied pH levels. Generally, as pH decreases, the limiting current density tends to rise. Moreover, the overall behavior of the current-voltage characteristics and overpotential remains consistent across the entire pH range. Nonetheless, the data in Fig. 3 indicates that the rate of increase in limiting current density per concentration increment is more pronounced at pH levels 1 and 2 compared to pH levels 3 and 4.5. This phenomenon can be attributed to the prevalence of hydrogen and nitrate ions in the acidified solutions, contributing significantly to charge transfer within the electrodialysis cell. Due to the logarithmic nature of the pH scale, there exists an order of magnitude difference in proton concentration between pH 1 and 2, as well as between pH 2 and 3 [64]. At pH 1, the proton concentration approximates 100 mM, exceeding the silver concentration by a factor of 10. Additionally, the mobility of hydrogen ions within the CEM matrix surpasses that of silver ions. Okada et al. [13,65] measured the membrane transport number of hydrogen versus other cations in Nafion 117 and found that the current was preferentially transported by hydrogen in a manner that is nonlinear in terms of the hydrogen fraction compared to other cations inside the membrane.

The extrapolations drawn from the plots displayed in Fig. 3 reveal that the intersection points with the y-axis occur at the origin for silver nitrate solutions without pH adjustment and at pH 2. In contrast, for nitric acid solutions at pH 1, the curve intersects the y-axis at 115 A/m^2.

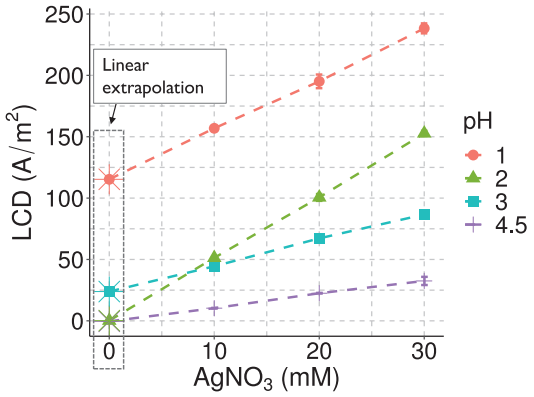

Fig. 2. Figures for determining the limiting current density using the boundary-layer method for three levels of silver nitrate concentration at pH 1: the electric potential is plotted as a function of the current density (a), the overpotential ΔE^{CP} is determined as the current-voltage characteristic's deviation from linearity (b), and finally, the ratio of membrane surface activity to bulk activity is determined by inserting ΔE^{CP} into the Nernst equation (Eq. (1)). The limiting current density is reached by definition once $\frac{a_i^{surf}}{a_i^{bulk}} < 0.01$. Full and hollow symbols of the same color represent repetitions at identical experimental conditions.

These intersection points mirror the variations in hydrogen concentration. When the silver nitrate concentration approaches zero, the solution lacks ions that facilitate charge transportation across the cell under neutral pH conditions. However, when the solution is acidified, protons become accessible for conveying charge across the cell, even without the presence of silver nitrate. At pH level 3, the intersection point suggests a limiting current density of 23.85 A/m^2 for a silver nitrate concentration of 0 mM. This contradicts the expectation that the limiting current density should be lower for pH 3 than for pH 2, given the heightened availability of protons and nitrate at the lower pH. The results for the linear extrapolation at pH 3 indicate that a linear relationship between the silver nitrate concentration and the limiting current density might not apply to silver nitrate concentrations between zero and 10 mM. However, experiments at 0 mM silver nitrate have not been carried out, as they hold no utility for the experiments performed in this study. For the desalination experiments, mixtures of 10 mM silver nitrate and 10 mM copper nitrate were prepared. As depicted in Fig. 3, the limiting current densities at pH 2 and 3 exhibit striking proximity for the 10 mM silver nitrate concentration. However, the increase in limiting current density demonstrates a steeper trajectory at pH 2 as the silver nitrate concentration rises. Consequently, despite the heightened availability of hydrogen and nitrate ions at the lower pH level - implying a greater portion of the current is allocated to the transport of these ions - comparable operational currents were employed for the desalination experiments conducted at pH 2 and 3. To comprehend the impact of the nitric acid addition on the competitive transport between silver and hydrogen, it is essential to conduct a more comprehensive examination of ion transport through both the CEM and AEM. Replicating the experiments while using different types of acids to modify the pH could give insight into the contribution of the anion transport to the limiting current density.

3.2. Desalination

Fig. 4 shows the silver removal, copper leakage, and electric potential during the electrodialysis process using equimolar mixtures of silver nitrate and copper nitrate at varying pH levels. The experiments were conducted for a duration of two hours or until the potentiostat's maximum electric potential limit was exceeded. Fig. 4c illustrates that, for pH levels between 1 and 3, the experiments were terminated before the full two-hour mark. The rapid rise in electric potential can be attributed to the depletion of ions, resulting in an increased resistance within the electrolyte. At pH 4.5, the electric potential exceeded 4 V.

Remarkably, at pH 3, the voltage exhibited an almost 4 V surge within the initial 10 min of treatment, compelling the halt of the experiment after 30 min, with 70 % of silver ions depleted from the silver-depleted compartment. The swift elevation in electric potential, despite a substantial presence of silver ions left in the silver-depleted compartment, implies that at the drawn current, the rate of transport across the cell limited the pace of charge transfer. Fig. 5a supports this by unveiling a notably higher transport rate at pH 3 compared to the other pH levels. At pH levels 1 and 2, silver removal was around 90 % after 104 and 70 min, respectively. A 96 % silver removal was achieved at pH 4.5 after 120 min. The copper leakage, illustrated in Fig. 4b, was approximately 20 % for pH levels 1, 2, and 4.5, with the lowest copper leakage of 13 % occurring at pH 3. This behavior corresponds well with the simultaneously reduced silver recovery at pH 3 and the relatively short duration of the experiment. Generally, higher copper leakage can be anticipated at increased current densities, as a greater number of copper ions could breach the charge barrier of the mCEMs. This observation aligns with findings from multiple studies highlighting the influence of current density on the selectivity between monovalent and divalent cations [17–22].

Interestingly, the plots in Fig. 4 do not follow a clear trend as functions of pH. The desalination experiments lasted longest at pH 4.5 and 1, followed by pH 2 and 3. It is hypothesized that this is caused by the

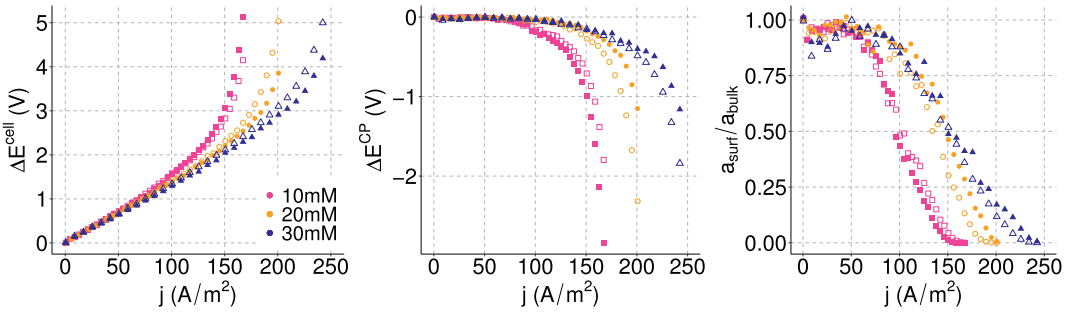

(a) current density-voltage curves (b) overpotential (c) activity ratio

Fig. 3. Limiting current density (LCD) versus silver nitrate concentration at pH 1, 2, 3, and 4.5. Values at 0 mM silver nitrate concentration are found by linear extrapolation.

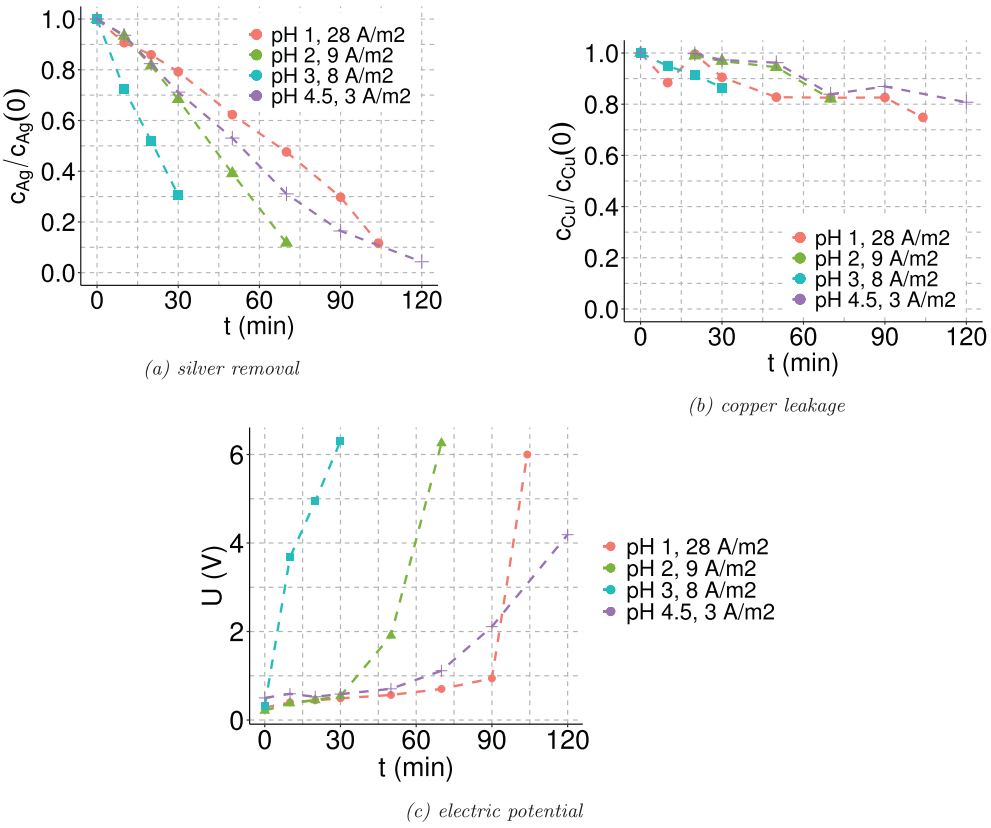

(a) silver removal (b) copper leakage

(c) electric potential

Fig. 4. Silver removal (a), copper leakage (b), and electric potential (c), as functions of time during electrodialysis of 10 mM equimolar mixtures of silver nitrate and copper nitrate at different pH levels. The current density was set to 20 % of the limiting current density.

contribution of the added nitric acid to the limiting current density. As described above, the mobility of hydrogen in the CEM is larger than that of the other available cations. Furthermore, the availability of nitrate increases with the addition of acid. Therefore, the limiting current density increases compared to the solutions at pH 4.5, where no nitric acid was added. The limiting current density experiments lasted relatively short, and it can be assumed that no ionic species were depleted in either batch during the testing. However, when performing desalination experiments, the hydrogen, which contributes significantly to the charge transfer, might be depleted during the first minutes of desalination at pH 3. The mobility of the remaining silver and copper cations might be too low to maintain the same rate of charge transfer, leading to a surge in electric potential. Hence, the silver removal and increase in electric potential over time follow the hydrogen and nitrate availability for the acidified solutions. At pH 4.5, there is no influence of additional hydrogen and nitrate in the limiting current density measurement, and the desalination can proceed until close to the complete depletion of silver. The initial ratio of drawn current to limiting current could be preserved by implementing dynamic regulation of the current. Continuous or multi-stage operation of the electrodialysis cell would have a similar effect [66].

For the purpose of evaluating performance, key metrics were computed as averages over the treatment duration. These metrics include the ionic flux of silver, the separation efficiency for silver over copper, the specific energy consumption per mol of silver removed from the silver-depleted compartment, and the energy efficiency. The outcomes are depicted in Fig. 5. Due to adjusting the operating current density to the limiting current density for silver in each respective solution, similar silver fluxes were expected across the different pH levels. This is true for pH levels 1, 2, and 4.5 with fluxes between 2.02 and 2.5

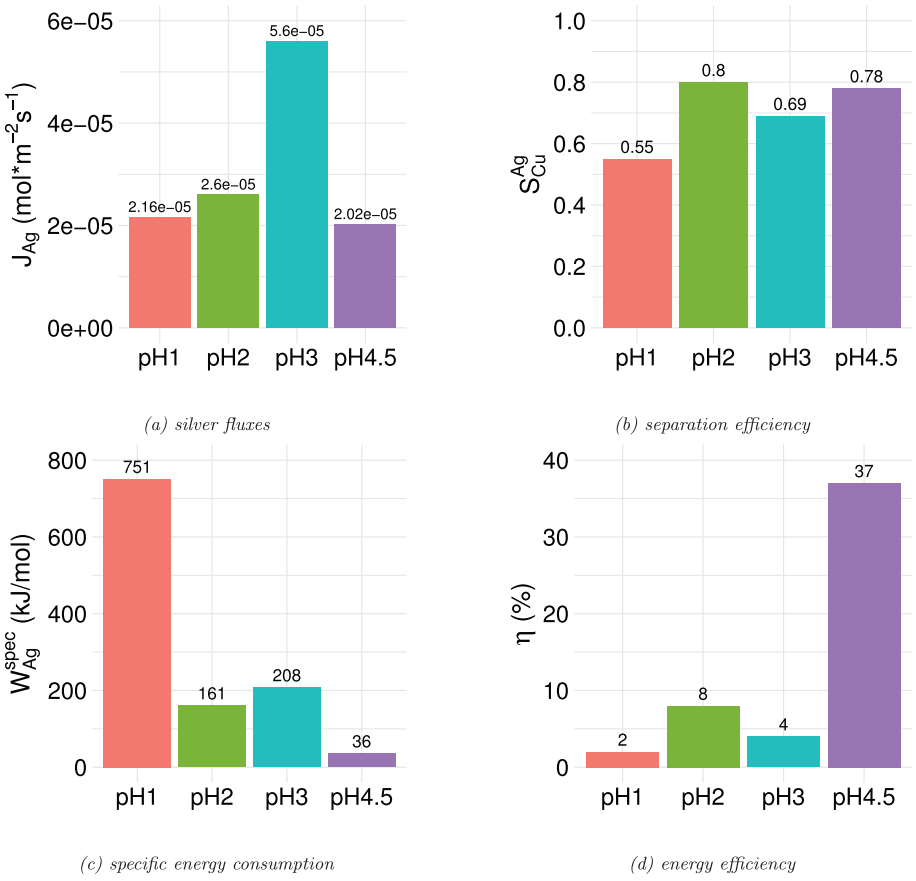

Fig. 5. The ionic flux of silver (a), separation efficiency for silver over copper (b), specific energy consumption per mol of silver removed from the silver-depleted batch (c), and energy efficiency (d), for electrodialysis of 10 mM equimolar mixtures of silver nitrate and copper nitrate at different pH levels, were calculated as average over the treatment time.

$mol \cdot m^{-2} \cdot s^{-1}$. However, the desalination experiment conducted at pH 3 displays a significantly elevated flux of 5.6 $mol \cdot m^{-2} \cdot s^{-1}$. The elevated silver flux at pH 3 can be attributed to the observation detailed in Section 3.1, where it was noted that the limiting current densities at pH levels 2 and 3 exhibit close similarity, despite a significant order of magnitude difference in proton concentration. In consequence, the desalination experiments at pH 2 and 3 were carried out with comparable current levels, despite the presence of a significantly higher concentration of nitrate and hydrogen ions in the solution at pH 2, contributing to charge transport. Therefore, at pH 3 a greater amount of charge is devoted to facilitating the transportation of silver, resulting in a heightened ionic flux. Notably, the data for pH 3 do not conform to the trend of decreasing specific energy consumption for silver removal with rising pH (as shown in Fig. 5c), nor to the trend of increased energy efficiency with higher pH (as illustrated in Fig. 5d). The separation efficiency, depicted in Fig. 5b, exhibits the lowest value at pH 1 (55 %), followed by pH 3 (69 %), pH 4.5 (78 %), and pH 2 (80 %). While the experiments conducted at pH 2 and 4.5 exhibit a similar silver flux and separation efficiency, experiments at pH 4.5 excel in terms of energy consumption, as evidenced by Fig. 5c and d. At pH 1, a total energy input of 751 kJ was required per mol of silver removed from the silver-depleted compartment. This requirement decreased to 161 kJ/mol at pH 2 and further down to 36 kJ/mol at pH 4.5. The energy efficiency showed an increase from values ranging between 2 % and 8 % at pH levels 1 to 3, to a notable 37 % at pH 4.5. The diminished energy efficiency observed in pH-adjusted solutions can be attributed to the presence and enhanced mobility of hydrogen. Energy efficiency is defined as the change in the chemical potential of silver across the membranes divided by the expended energy, as outlined in Eq. (4). Both copper leakage and hydrogen transport contribute negatively to energy efficiency. The analysis of energy consumption across the four pH levels suggests a significant advantage in raising the pH of acidic feed solutions in the context of electrodialysis.

Performing mass balance calculations for both silver and copper between the silver-depleted and silver-enriched batches highlighted a consistent phenomenon: a portion of the metals extracted from the silver-depleted solution did not make their way to the silver-enriched solution in each experiment. The proportions of silver and copper that were withdrawn from the silver-depleted solution but could not be traced in the silver-enriched solution are illustrated in Fig. 6. While the metal concentrations identified in the rinse solutions were negligible, it is anticipated that the primary share of the unaccounted substances has either formed precipitates in the solution, been deposited onto the surfaces of the membranes, or adsorbed within the matrices of the membranes themselves. Visual examination revealed the presence of precipitates on the membranes, with a notably more pronounced occurrence on the surfaces of the AEMs. Furthermore, the AEMs positioned closest to the electrodes exhibited the most significant impact, which could stem from the sulfate contained in the rinse solutions. The formation of sulfate salts can be mitigated by replacing the rinse solution. A substantial portion of the precipitate could be removed through scrubbing. Fig. 7a presents an overview of the silver and copper salts that could form within the studied system, and their solubility as a function of the solution pH. Evidently, solubility is constant over the whole pH range for nitrate salts and increases with decreasing pH for other salts. Yet, at pH levels 1 and 3, as much as 17 % and 16 % of silver, and 9 % and 15 % of copper, respectively, were missing from the silver-enriched compartment. For experiments conducted at pH 2 and 4.5, the

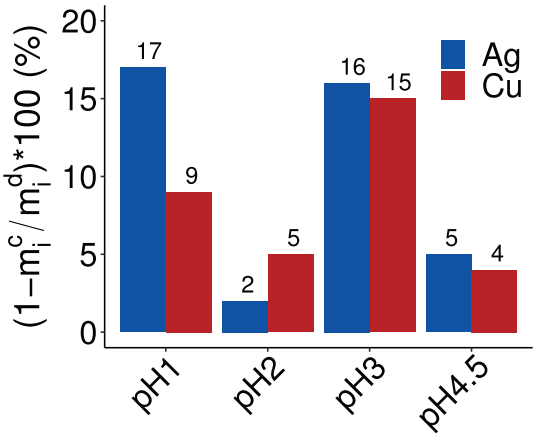

Fig. 6. Percentage of the dissolved silver and copper removed from the silver-depleted batch, that could not be traced in the silver-enriched batch. m_i^d and m_i^c are amounts of substances in the silver-depleted and silver-enriched batches, respectively. m_i was corrected for amounts of substance removed due to sampling.

missing quantities were notably lower: 2 % and 5 % for silver, and 5 % and 4 % for copper, respectively. The outcomes of the species distribution simulation are presented in Fig. 7b. The assessment indicates that silver and copper are predominantly present as Ag^+ and Cu^{2+} across the tested pH range.

At pH 1, approximately 5.5 % of the silver is likely to exist in the form of $AgNO_3$, which is more than twice the proportion observed at higher pH levels. A similar pattern emerges for copper, where roughly 12 % is expected to form $CuNO_3^+$ at pH 1, gradually decreasing to approximately 5 % at pH 2 and above. When the pH is raised to 4.5, there may be a minimal initiation of copper hydroxide species, each accounting for less than 0.1 %. The elevated presence of nitrate salts at pH 1 can be attributed to the nitrate abundance at this condition. The deviation from the mass balance of dissolved species observed at pH 1 (see Fig. 6) can thus be linked to the increased prevalence of nitrate species. Furthermore, the formation of $CuNO_3^+$ may offer an explanation for the reduced separation efficiency observed at pH 1 (see Fig. 5b). $CuNO_3^+$ is a monovalent cation and can, therefore, migrate through the mCEM. However, due to size exclusion, the transport rate of $CuNO_3^+$ is expected to be significantly slower compared to Ag^+ [11]. This slower transport rate can lead to the accumulation of $CuNO_3^+$ within the membrane. In evaluating the long-term stability of the membranes in this procedure, it is imperative to explore the degree to which cations, trapped within or on the membranes, undergo adsorption into the membrane matrix or precipitate. While adsorption is a dynamic process with a saturation point, precipitation can continually rise, resulting in elevated resistance and reduced permeability.

The significant deviation from the mass balance of dissolved species observed at pH 3 suggests that pH is not the sole influencing factor on the extent of precipitation. To explore whether alterations in the solution's pH influenced the surface charge of the CXP-S membrane and, consequently, the interaction between the membrane surface and metal ions, dye staining experiments were carried out. The detailed procedure is outlined in Appendix B. In Fig. B.1, the color intensity of the CXP-S membrane following exposure to methylene blue dye at various pH levels is displayed. Consistent color intensity values were observed for the stained CXP-S membrane across the pH range, suggesting resembling absorption of dye molecules. Evidently, the membrane maintained a stable surface charge over a range of pH environments, indicating that the membrane's functional groups were capable of dissociating effectively. It can be concluded that the electrostatic interactions between the membrane surface and metal ions remained constant under varying feed pH conditions. Therefore, it is reasonable to assume that the discrepancies in silver and copper removal and recovery at different pH levels were primarily driven by process conditions rather than structural changes in the membrane. As previously discussed, the estimated limiting current density for pH 3 may only remain valid as long as there are sufficient H^+ and NO_3^+ ions in the solution for charge transport. Once these ions are depleted, the transport rate of the remaining ions may be insufficient to balance the rate of charge transfer at the electrodes. When the limiting current is exceeded, secondary reactions, such as water splitting, can result in notable fluctuations in species concentrations and solution pH levels at the surfaces of the membranes, particularly at AEMs [71]. Elevated pH levels at the membrane surfaces can potentially induce the formation and precipitation of hydroxide species. Hydroxide ions can also stem from water electrolysis taking place within the electrode compartments. Additionally, uneven distribution of electric potential and locally elevated current densities can trigger water splitting at the membrane surfaces [72–76]. Factors such as membrane surface undulations, membrane clogging, and even scaling itself can contribute to such uneven potentials [77]. A comprehensive investigation of these phenomena by monitoring pH changes at the membrane surfaces during the experiment and analyzing the composition of the copper and silver species retained within the membrane is a relevant direction for future work. To facilitate the upscaling of the technology, it becomes crucial to investigate the long-term stability of the membranes and viable cleaning

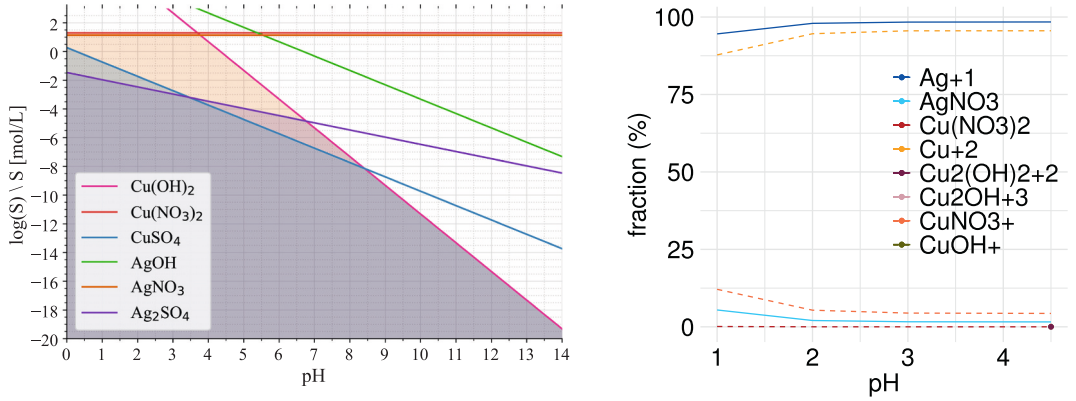

(a) Solubility plot *(b) Species distribution*

Fig. 7. (a) Solubility chart for the salts that may precipitate within the studied system. The solubility is represented as logarithmic values. Solubility product constants (K_{sp}) and acid dissociation constants (K_a) to generate the solubility plots were taken from [67–69]. (b) Speciation distribution for silver and copper in the feed solution at different pH levels. The copper hydroxide species were only present at pH level 4.5 and to a very small extent which makes them difficult to identify in the plot.

procedures. Applying a pulsed electric field may help mitigate membrane scaling and preserve high selectivity at elevated current densities [17,78]. Moreover, tailored membrane materials and designs could alleviate the extent of scaling. The combined optimization of both the membrane and the process holds the promise of rendering this process viable for solution purification in the hydrometallurgical industry.

4. Conclusions

In this study, the use of electrodialysis with monovalent-selective cation exchange membranes (mCEMs) was explored for the treatment of copper-contaminated effluent from silver recovery processes. The primary focus was on investigating how pH influenced the process performance. Hydrometallurgical solutions are typically characterized by low pH levels. Due to their high mobility within CEMs, hydrogen ions bear a significant portion of the charge and therefore elevate the energy requirements in electrodialysis. Correspondingly, the limiting current density was more elevated for solutions with lower pH. The desalination experiments involved treating equimolar solutions of 10 mM silver nitrate and copper nitrate at four distinct pH levels spanning from 1 to 4.5. The experiment at pH 3 was stopped at 30 % silver removal due to excessive electric potential. By configuring the operational current in relation to the limiting current, comparable outcomes were attained for the silver flux, copper leakage, and separation efficiency at pH 1, 2, and 4.5. This emphasizes the pivotal role of limiting current density as a controlling parameter in the electrodialysis process. The pH exerted a significant impact on the energy demand for silver removal, dropping from 751 kJ/mol at pH 1 to 36 kJ/mol at pH 4.5. Concurrently, the energy efficiency improved from 2 % at pH 1 to 37 % at pH 4.5. Electrodialysis with mCEMs for the recovery of silver from copper-contaminated effluents achieved up to 80 % silver separation efficiency with an energy efficiency of 37 %. These results reveal a large potential for electrodialysis as a technology to refine such effluents, though case-specific assessment is crucial. In particular, low pH has a negative influence on the energy efficiency, suggesting potential benefits of adjusting the solution pH prior to electrodialysis treatment. However, membrane scaling poses a challenge that should be further addressed in future work.

CRediT authorship contribution statement

Pauline Zimmermann: Conceptualization, Methodology, Formal analysis, Validation, Investigation, Writing - original draft, Visualization.

Kristin Wahl: Investigation, Writing – Review & editing.

Önder Tekinalp: Methodology, Writing - Review & editing.

Simon Birger Byremo Solberg: Methodology, Writing - Review & editing.

Liyuan Deng: Supervision, Writing - Review & editing.

Øivind Wilhelmsen: Supervision, Writing - Review & editing.

Odne Stokke Burheim: Conceptualization, Supervision, Writing - Review & editing.

All authors have read and agreed to the published version of the manuscript.

Declaration of competing interest

Pauline Zimmermann reports equipment, drugs, or supplies was provided by KA Rasmussen AS.

Data availability

Data will be made available on request.

Acknowledgements

The authors acknowledge the financial support from the Research Council of Norway (RCN-BIA) through the PRICE project (No. 294543). The authors also thank L. D. Biagi and other colleagues from K.A. Rasmussen AS for technical assistance. ØW acknowledges funding from the Research Council of Norway (RCN), the Center of Excellence Funding Scheme, Project No. 262644, PoreLab.

Appendix A. Limiting current density

Figs. A.1 to A.3 plot the current-voltage characteristics, overpotential, and activity ratio at the membrane surface and in the bulk solution for silver nitrate solutions of 10 mM, 20 mM, and 30 mM at pH 2, 3, and 4.5. Each experiment was repeated once, and the full and hollow symbols represent repetitions at the same conditions. The data were used to estimate the limiting current densities for the specific pH levels and silver nitrate concentrations.

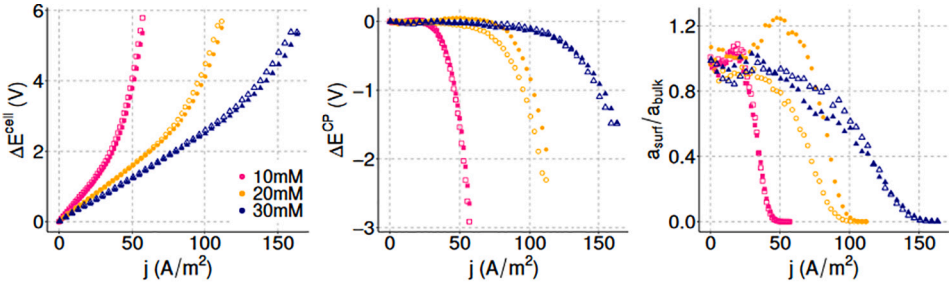

Fig. A.1. Determination of the limiting current density for three levels of silver nitrate concentration at pH 2.

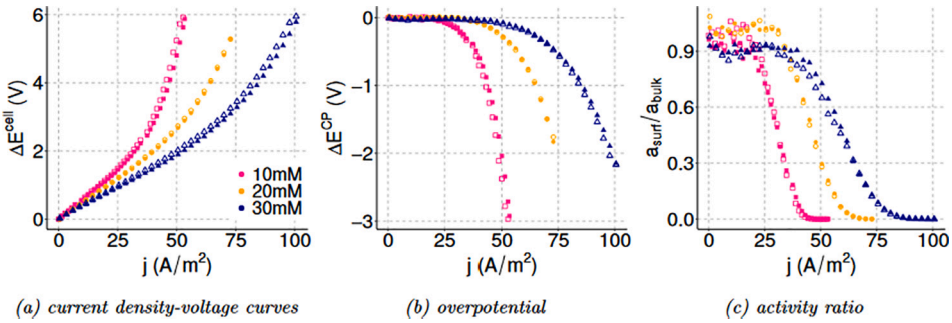

Fig. A.2. Determination of the limiting current density for three levels of silver nitrate concentration at pH 3.

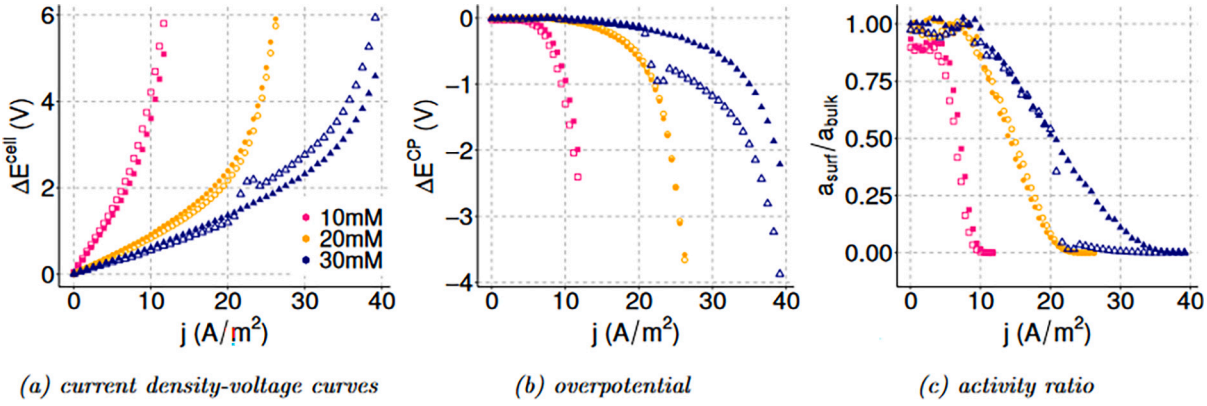

Fig. A.3. Determination of the limiting current density for three levels of silver nitrate concentration at pH 4.5.

Appendix B. Color intensity

The surface charge of an ion-exchange membrane plays a crucial role in determining its ion flux, as it exerts electrostatic forces on the ions and influences the distribution of ions adjacent to the membrane. Variations in the pH of the surrounding solution can induce shifts in the surface charge of such membranes. To investigate whether adjustments in the solution's pH impacted the surface charge of the CXP-S membrane and, consequently, the interplay between the membrane surface and metal ions, dye staining experiments were conducted using methylene blue dye, following the procedure described in [60]. The membranes were submerged in 10 mM methylene blue solutions at pH levels of 4.5, 3, 2, or 1 for a duration of 15 min. Methylene blue exhibits an isoelectric point at approximately pH 8, and in solutions with pH levels lower than 8, it assumes a positively charged state [61]. Following the staining process, the membranes were thoroughly rinsed with deionized water until the rinse water exhibited no further coloration, thereby ensuring the removal of loosely adhered dye molecules from the membrane's surface. Quantification of the color intensity was accomplished using a spectrometer in conjunction with AvaSoft software. Fig. B.1 shows the color intensity of the CXP-S membrane after exposure to methylene blue dye at different pH levels. The reference membrane, which was not subjected to the dye solution, exhibited a color intensity of 19 ± 0.8. Staining with methylene blue at various pH levels led to reduced color intensities, implying dye attachment to the membrane surface. Consistent color intensity measurements were noted for the stained CXP-S membrane at various pH levels, suggesting a uniform absorption of dye molecules.

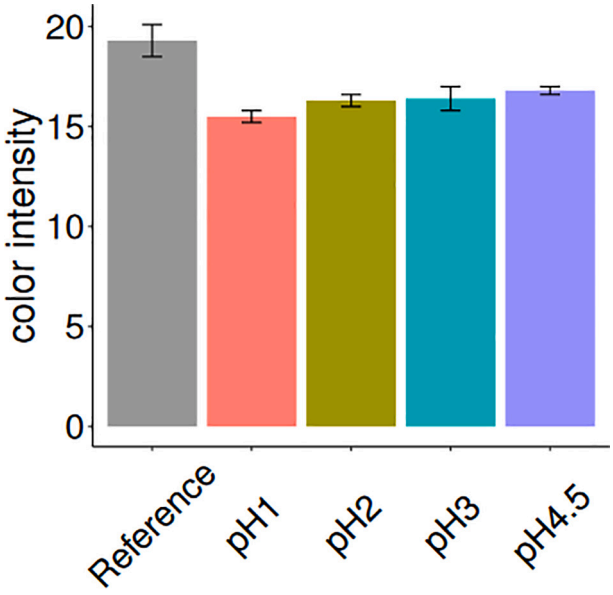

Fig. B.1. Color intensity values of CXP-S CEMs following exposure to methylene blue at various pH values. Lower color intensity corresponds to a greater methylene blue dye adsorption.

References

[1] A.T. Nakhjiri, H. Sanaeepur, A.E. Amooghin, M.M.A. Shirazi, Recovery of precious metals from industrial wastewater towards resource recovery and environmental sustainability: A critical review, Desalination 527 (2022), 115510.

[2] K. Yang, X. Li, J. Cui, M. Zhang, Y. Wang, Z. Lou, W. Shan, Y. Xiong, Facile synthesis of novel porous graphene-like carbon hydrogel for highly efficient recovery of precious metal and removal of organic dye, Appl. Surf. Sci. 528 (2020), 146928.

[3] S. Syed, Silver recovery aqueous techniques from diverse sources: hydrometallurgy in recycling, Waste Manag. 50 (2016) 234–256.

[5] W. Kunda, T. Etsell, Recovery of silver from x-ray film, in: Precious Metals, Metchem Research, Boulder, CO, 1985, pp. 289–304.

[6] Y. Ding, S. Zhang, B. Liu, H. Zheng, C.-C. Chang, C. Ekberg, Recovery of precious metals from electronic waste and spent catalysts: A review, Resour. Conserv. Recycl. 141 (2019) 284–298.

[7] J. Sitko, Analysis of selected technologies of precious metal recovery processes, in: Multidisciplinary Aspects of Production Engineering 2, 2019.

[8] H. Strathmann, Electrodialysis, a mature technology with a multitude of new applications, Desalination 264 (3) (2010) 268–288.

[9] E. Korngold, K. Kock, H. Strathmann, Electrodialysis in advanced waste water treatment, Desalination 24 (1–3) (1977) 129–139.

[10] T. Luo, S. Abdu, M. Wessling, Selectivity of ion exchange membranes: A review, J. Membr. Sci. 555 (2018) 429–454.

[11] Ö. Tekinalp, P. Zimmermann, S. Holdcroft, O.S. Burheim, L. Deng, Cation exchange membranes and process optimizations in Electrodialysis for selective metal separation: A review, Membranes 13 (6) (2023) 566.

[12] F. Roghmans, E. Evdochenko, M. Martıé-Calatayud, M. Garthe, R. Tiwari, A. Walther, M. Wessling, On the permselectivity of cation-exchange membranes bearing an ion selective coating, J. Membr. Sci. 600 (2020), 117854.

[13] T. Okada, H. Satou, M. Okuno, M. Yuasa, Ion and water transport characteristics of perfluorosulfonated ionomer membranes with H+ and alkali metal cations, J. Phys. Chem. B 106 (6) (2002) 1267–1273, https://doi.org/10.1021/jp013195l.

[14] S.B. Solberg, P. Zimmermann, Ø. Wilhelmsen, R. Bock, O.S. Burheim, Analytical treatment of ion-exchange permselectivity and transport number measurements for high accuracy, J. Membr. Sci. 685 (2023), 121904.

[15] Ö. Tekinalp, P. Zimmermann, O.S. Burheim, L. Deng, Designing monovalent selective anion exchange membranes for the simultaneous separation of chloride and fluoride from sulfate in an equimolar ternary mixture, J. Membr. Sci. 666 (2023), 121148.

[16] P. Zimmermann, S.B.B. Solberg, Ö. Tekinalp, J.J. Lamb, Ø. Wilhelmsen, L. Deng, O. S. Burheim, Heat to hydrogen by RED—reviewing membranes and salts for the RED heat engine concept, Membranes 12 (1) (2021) 48.

[17] A. Gorobchenko, S. Mareev, V. Nikonenko, Mathematical modeling of monovalent Permselectivity of a bilayer ion-exchange membrane as a function of current density, Int. J. Mol. Sci. 23 (9) (2022) 4711.

[18] D. Golubenko, A. Yaroslavtsev, Effect of current density, concentration of ternary electrolyte and type of cations on the monovalent ion selectivity of surface-sulfonated graft anion-exchange membranes: modelling and experiment, J. Membr. Sci. 635 (2021), 119466.

[19] W. Zhang, M. Miao, J. Pan, A. Sotto, J. Shen, C. Gao, B. Van der Bruggen, Separation of divalent ions from seawater concentrate to enhance the purity of coarse salt by electrodialysis with monovalent-selective membranes, Desalination 411 (2017) 28–37.

[20] T. Rottiers, J. De Staelen, B. Van der Bruggen, L. Pinoy, Permselectivity of cationexchange membranes between different cations in aqueous alcohol mixtures, Electrochim. Acta 192 (2016) 489–496.

[21] W. Wang, R. Liu, M. Tan, H. Sun, Q.J. Niu, T. Xu, V. Nikonenko, Y. Zhang, Evaluation of the ideal selectivity and the performance of selectrodialysis by using TFC ion exchange membranes, J. Membr. Sci. 582 (2019) 236–245.

[22] P. Xu, M. Capito, T.Y. Cath, Selective removal of arsenic and monovalent ions from brackish water reverse osmosis concentrate, J. Hazard. Mater. 260 (2013) 885–891.

[23] G. Chen, K. Wei, A. Hassanvand, B. Freeman, S. Kentish, Single and binary ion sorption equilibria of monovalent and divalent ions in commercial ion exchange membranes, Water Res. 175 (2020), 115681.

[24] Y.D. Ahdab, D. Rehman, et al., Brackish water desalination for greenhouses: improving groundwater quality for irrigation using monovalent selective electrodialysis reversal, J. Membr. Sci. 610 (2020), 118072.

[25] L. Firdaous, J.-P. Malériat, J.-P. Schlumpf, F. Quéméneur, Transfer of monovalent and divalent cations in salt solutions by electrodialysis, Sep. Sci. Technol. 42 (5) (2007) 931–948.

[26] A. Galama, G. Daubaras, O. Burheim, H. Rijnaarts, J. Post, Fractioning electrodialysis: a current induced ion exchange process, Electrochim. Acta 136 (2014) 257–265.

[27] A. Galama, G. Daubaras, O. Burheim, H. Rijnaarts, J. Post, Seawater electrodialysis with preferential removal of divalent ions, J. Membr. Sci. 452 (2014) 219–228.

[28] X.-Y. Nie, S.-Y. Sun, Z. Sun, X. Song, J.-G. Yu, Ion-fractionation of lithium ions from magnesium ions by electrodialysis using monovalent selective ion-exchange membranes, Desalination 403 (2017) 128–135.

[29] Y. Zhang, B. Van der Bruggen, L. Pinoy, B. Meesschaert, Separation of nutrient ions and organic compounds from salts in RO concentrates by standard and monovalent selective ion-exchange membranes used in electrodialysis, J. Membr. Sci. 332 (1–2) (2009) 104–112.

[30] B. Van der Bruggen, A. Koninckx, C. Vandecasteele, Separation of monovalent and divalent ions from aqueous solution by electrodialysis and nanofiltration, Water Res. 38 (5) (2004) 1347–1353.

[31] T. Rijnaarts, D.M. Reurink, F. Radmanesh, W.M. De Vos, K. Nijmeijer, Layer-by-layer coatings on ion exchange membranes: effect of multilayer charge and hydration on monovalent ion selectivities, J. Membr. Sci. 570 (2019) 513–521.

[32] S. Abdu, M.-C. Martıé-Calatayud, J.E. Wong, M. Garcıéa-Gabaldón, M. Wessling, Layer-by-layer modification of cation exchange membranes controls ion selectivity and water splitting, ACS Appl. Mater. Interfaces 6 (3) (2014) 1843–1854.

[33] N. White, M. Misovich, A. Yaroshchuk, M.L. Bruening, Coating of Nafion membranes with polyelectrolyte multilayers to achieve high monovalent/divalent cation electrodialysis selectivities, ACS Appl. Mater. Interfaces 7 (12) (2015) 6620–6628.

[34] N. White, M. Misovich, E. Alemayehu, A. Yaroshchuk, M.L. Bruening, Highly selective separations of multivalent and monovalent cations in electrodialysis through Nafion membranes coated with polyelectrolyte multilayers, Polymer 103 (2016) 478–485.

[35] C. Cheng, N. White, H. Shi, M. Robson, M.L. Bruening, Cation separations in electrodialysis through membranes coated with polyelectrolyte multilayers, Polymer 55 (6) (2014) 1397–1403.
[36] Y. Zhu, M. Ahmad, L. Yang, M. Misovich, A. Yaroshchuk, M.L. Bruening, Adsorption of polyelectrolyte multilayers imparts high monovalent/divalent cation selectivity to aliphatic polyamide cation-exchange membranes, J. Membr. Sci. 537 (2017) 177–185.
[37] M. Ahmad, A. Yaroshchuk, M.L. Bruening, Moderate pH changes alter the fluxes, selectivities and limiting currents in ion transport through polyelectrolyte multilayers deposited on membranes, J. Membr. Sci. 616 (2020), 118570.
[38] D. Ding, A. Yaroshchuk, M.L. Bruening, Electrodialysis through nafion membranes coated with polyelectrolyte multilayers yields. 99% pure monovalent ions at high recoveries, J. Membr. Sci. 647 (2022), 120294.
[39] L. Yang, C. Tang, M. Ahmad, A. Yaroshchuk, M.L. Bruening, High selectivities among monovalent cations in dialysis through cation-exchange membranes coated with polyelectrolyte multilayers, ACS Appl. Mater. Interfaces 10 (50) (2018) 44134–44143.
[40] J.-M.A. Juve, F.M.S. Christensen, Y. Wang, Z. Wei, Electrodialysis for metal removal and recovery: A review, Chem. Eng. J. 435 (2022), 134857.
[41] P. Zimmermann, Ö. Tekinalp, L. Deng, K. Forsberg, Ø. Wilhelmsen, O. Burheim, Electrodialysis in hydrometallurgical processes, in: Rare Metal Technology 2020, Springer, 2020, pp. 159–167.
[42] K. Staszak, K. Wieszczycka, Recovery of metals from wastewater—state-of-the-art solutions with the support of membrane technology, Membranes 13 (1) (2023) 114.
[43] V. Schmidt, Electrochemical Process Engineering, John Wiley & Sons, Incorporated, 2014.
[44] A. Smara, R. Delimi, E. Chainet, J. Sandeaux, Removal of heavy metals from diluted mixtures by a hybrid ion-exchange/electrodialysis process, Sep. Purif. Technol. 57 (1) (2007) 103–110.
[45] A. Güvenc, B. Karabacakolu, Use of electrodialysis to remove silver ions frommodel solutions and wastewater, Desalination 172 (1) (2005) 7–17.
[46] M. Reig, X. Vecino, C. Valderrama, O. Gibert, J.-L. Cortina, Application of selectrodialysis for the removal of as from metallurgical process waters: recovery of cu and Zn, Sep. Purif. Technol. 195 (2018) 404–412.
[47] J. Lambert, M. Avila-Rodriguez, G. Durand, M. Rakib, Separation of sodium ions from trivalent chromium by electrodialysis using monovalent cation selective membranes, J. Membr. Sci. 280 (1–2) (2006) 219–225.
[48] C. Vallois, P. Sistat, S. Rouald'es, G. Pourcelly, Separation of H+/Cu2+ cations by electrodialysis using modified proton conducting membranes, J. Membr. Sci. 216 (1–2) (2003) 13–25.
[49] T.Z. Sadyrbaeva, Separation of palladium (II) and platinum (IV) by bulk liquid membranes during electrodialysis, Separation Science and Technology 41 (14) (2006) 3213–3228.
[50] T.Z. Sadyrbaeva, Separation of platinum (IV) and iron (III) with liquid membranes under electrodialysis conditions, Russ. J. Appl. Chem. 76 (2003) 76–79.
[51] H. Rezaei, H. Abdollahi, S. Ghassa, Recovery of gold ions from wastewater using a three-compartment electrodialysis separation system, Int. J. Environ. Sci. Technol. 20 (5) (2023) 4827–4838.
[52] A. Cherif, A. Elmidaoui, C. Gavach, Separation of ag+, Zn2+ and Cu2+ ions by electrodialysis with monovalent cation specific membrane and EDTA, J. Membr. Sci. 76 (1) (1993) 39–49.
[53] S. Frioui, R. Oumeddour, S. Lacour, Highly selective extraction of metal ions from dilute solutions by hybrid electrodialysis technology, Sep. Purif. Technol. 174 (2017) 264–274.
[54] ASTOM, Products Catalogue, url: http://www.astom-corp.jp/en/catalog/pdf/Astom_Products_Catalogue.pdf?20221003. visited on 10/08/2023.
[55] P. Zimmermann, Ö. Tekinalp, S.B.B. Solberg, O. Wilhelmsen, L. Deng, O. S. Burheim, Limiting current density as a selectivity factor in electrodialysis of multi-ionic mixtures, Desalination 558 (2023), 116613.
[56] K. Kontturi, L. Murtomäki, J.A. Manzanares, Ionic transport processes in electrochemistry and membrane science, Oxford University Press Inc., 2008, https://doi.org/10.1093/acprof:oso/9780199533817.001.0001.
[57] C.B. Smith, K.E. Parmenter, Chapter 7 - energy analysis, in: C.B. Smith, K. E. Parmenter (Eds.), Energy Management Principles, Second edition, Elsevier, Oxford, 2016, pp. 95–123, https://doi.org/10.1016/B978-0-12-802506-2.00007-0.
[59] M. Asraf-Snir, J. Gilron, Y. Oren, Gypsum scaling of anion exchange membranes in electrodialysis, J. Membr. Sci. 520 (2016) 176–186.
[60] Ö. Tekinalp, S.A. Altinkaya, Development of high flux nanofiltration membranes through single bilayer polyethyleneimine/alginate deposition, J. Colloid Interface Sci. 537 (2019) 215–227.
[61] E. Saputra, R. Saputra, M. Nugraha, R. Irianty, P. Utama, Removal of Methylene Blue from aqueous solution using spent bleaching earth, in: IOP Conference Series: Materials Science and Engineering, 1 345, IOP Publishing, 2018, p. 012008.
[62] Gustafsson, Petter. Visual MINTEQ ver. 3.1 (released 2014). Version 3.1. https://vminteq.lwr.kth.se/. Nov. 26, 2020.
[63] J.F. Pankow, Aquatic Chemistry Concepts, CRC Press, 2019.
[64] R. Bates, Determination of PH: Theory and Practice, Wiley-Interscience publication. Wiley, 1973.
[65] T. Okada, N. Nakamura, M. Yuasa, I. Sekine, Ion and water transport characteristics in membranes for polymer electrolyte fuel cells containing H+ and Ca2+ cations, J. Electrochem. Soc. 144 (8) (1997) 2744.
[66] L. Wang, C. Violet, R.M. DuChanois, M. Elimelech, Derivation of the theoretical minimum energy of separation of desalination processes, J. Chem. Educ. 97 (12) (2020) 4361–4369, https://doi.org/10.1021/acs.jchemed.0c01194.
[67] B.G. Steen, Gyldendals tabeller og formler i kjemi, Gyldendal Norsk Forlag AS, 2010.
[68] W.M. Haynes, CRC Handbook of Chemistry and Physics, CRC press, 2014.
[69] G.H. Aylward, T.J. Findlay, Datensammlung Chemie in SI-Einheiten, John Wiley & Sons, 2014.
[71] T. Belloň, Z. Slouka, Overlimiting behavior of surface-modified heterogeneous anion exchange membranes, J. Membr. Sci. 610 (2020), 118291.
[72] J. Krol, M. Wessling, H. Strathmann, Concentration polarization with monopolar ion exchange membranes: current–voltage curves and water dissociation, J. Membr. Sci. 162 (1–2) (1999) 145–154.
[73] R. Simons, Water splitting in ion exchange membranes, Electrochim. Acta 30 (3) (1985) 275–282.
[74] Y. Oda, T. Yawataya, Neutrality-disturbance phenomenon of membrane-solution systems, Desalination 5 (2) (1968) 129–138.
[75] V. Mavrov, W. Pusch, O. Kominek, S. Wheelwright, Concentration polarization and water splitting at electrodialysis membranes, Desalination 91 (3) (1993) 225–252.
[76] I. Rubinstein, E. Staude, O. Kedem, Role of the membrane surface in concentration polarization at ion-exchange membrane, Desalination 69 (2) (1988) 101–114.
[77] Y. Tanaka, Water dissociation in ion-exchange membrane electrodialysis, J. Membr. Sci. 203 (1–2) (2002) 227–244.
[78] N. Lemay, S. Mikhaylin, S. Mareev, N. Pismenskaya, V. Nikonenko, L. Bazinet, How demineralization duration by electrodialysis under high frequency pulsed electric field can be the same as in continuous current condition and that for better performances? J. Membr. Sci. 603 (2020), 117878.